Eur. Phys. J. B (2018) 91: 128
https://doi.org/10.1140/epjb/e2018-90166-9

THE EUROPEAN PHYSICAL JOURNAL B

Regular Article

Gradient-level and nonlocal density functional descriptions of Cu-Au intermetallic compounds*

Henrik Levämäki[1,a], Liyun Tian[1], Kalevi Kokko[2,3], and Levente Vitos[1,4,5]

[1] Applied Materials Physics, Department of Materials Science and Engineering, Royal Institute of Technology, Stockholm 100 44, Sweden
[2] Department of Physics and Astronomy, University of Turku, 20014 Turku, Finland
[3] Turku University Centre for Materials and Surfaces (MatSurf), Turku, Finland
[4] Institute for Solid State Physics and Optics, Wigner Research Centre for Physics, Hungarian Academy of Sciences, P.O. Box 49, 1525 Budapest, Hungary
[5] Department of Physics and Astronomy, Division of Materials Theory, Uppsala University, Box 516, 75121 Uppsala, Sweden

Received 13 March 2018 / Received in final form 25 April 2018
Published online 22 June 2018

Abstract. We use three gradient level and two nonlocal density functional approximations to study the thermodynamic properties of Cu-Au compounds. It is found that a well-designed gradient level approximation (quasi non-uniform approximation, QNA) reproduces the experimental equilibrium volumes and the formation energies of L12 and L10 phases. On the other hand, QNA predicts a non-existent β_2 phase, which can be remedied only when employing the nonlocal hybrid-level Heyd-Scuseria-Ernzerhof (HSE06) or Perdew-Burke-Ernzerhof (PBE0) approximations. Gradient-level approximations lead to similar electronic structures for the Cu-Au compounds whereas hybrids shift the *d*-band towards negative energies and account for the complex *d*-*d* hybridization more accurately.

1 Introduction

Density functional theory (DFT) [1–3] has been established to be able to give an accurate description of the electronic structure of matter in a wide range of scenarios. There are, however, many interesting situations that expose the weaknesses of currently popular DFT approximations [4]. In the realm of alloy theory one of the major challenges for DFT is the ability to predict accurate formation energies and phase stabilities that would even qualitatively agree with experimental findings [5–8]. One notable example is the Cu-Au binary alloy system for which the standard exchange-correlation (XC) approximations, the local density approximation (LDA) [2,9,10] and the semilocal Perdew-Burke-Ernzerhof (PBE) [11] generalized gradient approximation (GGA) [12–14], first of all predict formation energies that are too small in magnitude, by nearly a factor of two [5,6,8]. Another severe issue is that within (semi) local DFT the $CuAu_2$-β_2 phase is predicted to be so exothermic in relation to CuAu-$L1_0$ and $CuAu_3$-$L1_2$ phases that $CuAu_2$-β_2 on the semilocal level is a stable structure and $CuAu_3$-$L1_2$ unstable. From experimental point of view this is a conflict, because $CuAu_2$-β_2 has never been observed and $CuAu_3$-$L1_2$ has been suggested to be stable at low temperatures. Similar problems with the magnitudes of formation energies and the β_2 structure stability has recently been reported also for the Co-Pt system [7] and the authors of that paper speculate that related alloys, such as Fe-Pt, Ni-Pt, Fe-Ni, are likely to be plagued by the same or similar issues.

Recently, Zhang et al. have shown that nonlocal hybrid functionals, such as the Heyd-Scuseria-Ernzerhof (HSE06, but hereafter just HSE) [15,16], can effectively fix both the formation energy and the phase stability problems in Cu-Au. They conclude that the observed improvements in formation energies are connected to improved hybrid-level lattice constants of Cu and Au. But the mechanism by which the HSE hybrid functional is able to fix the phase stability issue – and thereby make $CuAu_2$-β_2 unstable and $CuAu_3$-$L1_2$ stable – was not fully settled. The situation is made more interesting by the GGA-level quasi-non-uniform (QNA) scheme [17,18] which also produces very accurate Cu and Au lattice constants, and by connection much improved GGA-level Cu-Au formation energies [8]. Since QNA is not a hybrid-level functional, the question of how the mechanisms by which QNA and PBE0 produce improved formation energies might differ from one another is an interesting one.

In this paper we first briefly describe the QNA-GGA and hybrid-level PBE0 [19,20] and HSE approaches, which can all be used to obtain Cu-Au formation energies

* Contribution to the Topical Issue "Special issue in honor of Hardy Gross", edited by C.A. Ullrich, F.M.S. Nogueira, A. Rubio, and M.A.L. Marques.

[a] e-mail: hpleva@utu.fi

that are superior to those of LDA and PBE. Using these approaches we find that while the Cu-rich end of the formation energies are very similar between QNA and PBE0/HSE, the Au-rich end shows some key differences. Most importantly, PBE0 and HSE recover the experimentally correct phase stability, while on the QNA-GGA level the $CuAu_2$-β_2 phase remains stable. We also gain new insight into how hybrid functionals are able to rectify the Cu-Au the phase stability issue that is here seen to persists on the GGA and meta-GGA levels.

2 Methods

2.1 Projector-augmented wave calculations

Electronic structure calculations were performed with Vienna Ab initio Simulation Package (VASP) [21–23] and GPAW [24,25] DFT codes, which both made use of the projector-augmented wave (PAW) method [26,27]. The energy cutoff for the plane waves was 400 eV in VASP and 550 eV in GPAW. The Brillouin zones were sampled by Monkhorst-Pack scheme [28]. The sizes of the k-points meshes were chosen to be large enough to ensure good convergence. First self-consistent calculations were performed with VASP using the PBE XC functional and by allowing the lattice parameters and atomic positions to be relaxed. After PBE we performed the HSE and PBE0 hybrid VASP calculations in a non-self-consistent manner by performing one self-consistent iteration and by using the relaxed VASP PBE geometries and wavefunctions as the starting point. For QNA GPAW formation energies were computed both self-consistently and non-self-consistently (by evaluating the total energy using converged GPAW PBE density), and the electronic densities of states were computed self-consistently. The GPAW calculations were also performed using the relaxed VASP PBE geometries.

2.2 Exact muffin-tin orbitals calculations

The exact muffin-tin orbitals (EMTO) [29–32] method can be viewed as an improved screened Korringa-Kohn-Rostoker method [33], in which the exact one-electron potential is represented by large overlapping muffin-tin potential spheres. Random alloys, such as Fe-V and V-W in Figure 1, are efficiently simulated using EMTO with the help of the coherent potential approximation (CPA) [34,35] and the full charge density (FCD) technique [36,37]. Other recent EMTO applications vary from dynamical mean field theory [38] to investigating the nature of the GGA-level XC problems in binary alloy formation energies using the QNA scheme [8].

3 Exchange-correlation treatment

3.1 QNA-GGA

The QNA scheme was designed to improve the description of metallic bulk alloys and it is developed in response to the fact that on GGA level it is more or less impossible to have an XC functional that could yield sufficiently accurate ground-state equilibrium volumes – and equations of state in general – for all elements in the periodic table [39]. When calculating transition metal equilibrium volumes the so-called core-valence overlap region (CVOR) plays a key role [8,18,40–44]. However, many transition metals, e.g. Cu and V, have very similar electron densities n and reduced density gradients $s = |\nabla n|/[2(3\pi^2 n)^{1/3} n]$ within the CVOR [39]. As n and s are conventionally the only two pieces of information that a GGA functional has about any given system, it seems therefore practically impossible for any GGA to properly discern between different elements. For the GGA-level simulation of metallic alloys this poses a serious problem, because many important properties, such as volume (Fig. 1) and formation energy (Fig. 3), depend on how accurately the component elements of the alloy are described by the GGA functional. Recently it has been shown that on GGA level consistently accurate formation energies of binary alloys require an XC functional that is accurate for both component elements of the alloy; it is not enough to be accurate for just one component or the other [8].

In the QNA scheme the GGA-level problem is circumvented by utilizing the idea of subsystem functionals

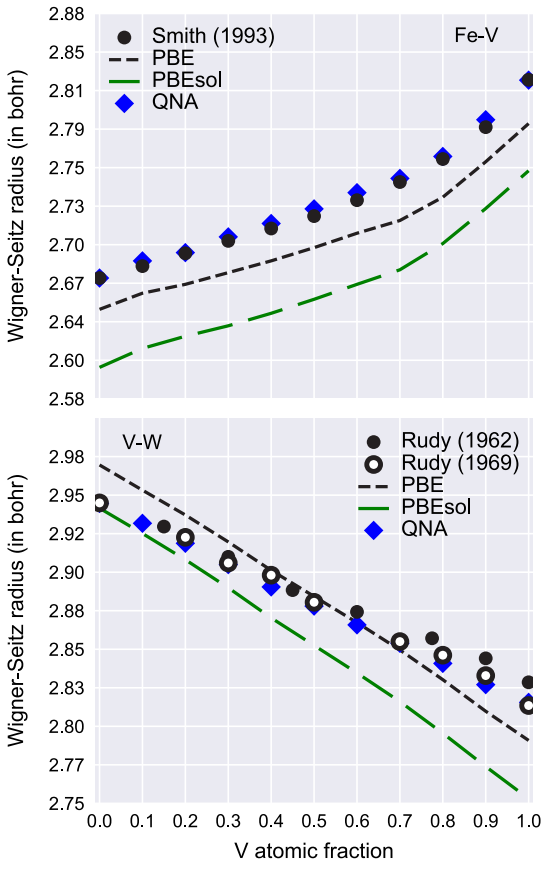

Fig. 1. Calculated EMTO-CPA PBE, PBEsol, QNA, and experimental Wigner-Seitz radii of Fe-V and V-W random binary alloys. Experimental data are represented by solid and filled circles [17].

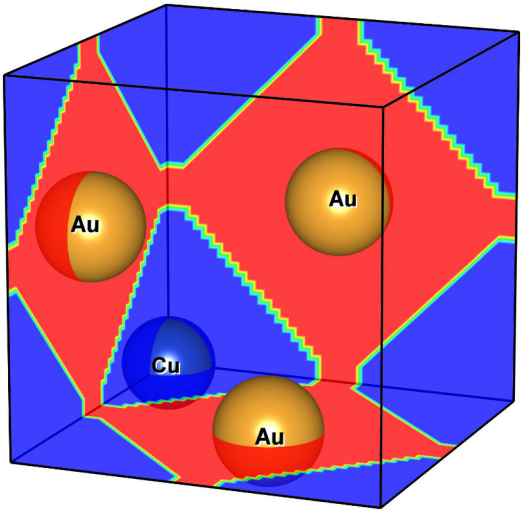

Fig. 2. Planar sections of space that has been divided into atom-centered non-overlapping Voronoi-type regions for $CuAu_3$-$L1_2$.

[45–48]. For each component of the alloy an element-specific, atom-centered subsystem XC functional is developed and then the total XC functional can be expressed as a superposition

$$E_{\mathrm{XC}}^{\mathrm{QNA}} = \sum_q \int_{\Omega_q} n(\mathbf{r}) \epsilon_{\mathrm{XC}}^{\mathrm{SF}_q}(\mathbf{r})\, d\mathbf{r} \qquad (1)$$

of the subsystem functionals $\epsilon_{\mathrm{XC}}^{\mathrm{SF}_q}$, which only act within the volume Ω_q of their own atomic site q. One way of implementing this idea in practice is to use the PBE functional form as a starting point and to find for each element optimal μ and β parameter values that are used by the PBE functional. Such optimal values have been reported in reference [18] for 25 transition metals.

For alloy calculations the QNA procedure solves the issue with the impossibility of designing a conventional GGA that would have sufficient accuracy for all component elements of alloys and compounds. In practice, real space has to be explicitly partitioned into atom-centered regions Ω_q to accommodate the calculation of QNA total XC energy, which is illustrated in Figure 2. The figure shows sharp Voronoi-type partitioning, which we have found to give accurate results, but such a choice technically introduces discontinuities between adjacent Voronoi-cells that have differently configured subsystem functionals. For the computation of the total QNA XC energy $E_{\mathrm{XC}}^{\mathrm{QNA}}$ the threat posed by the discontinuities is minor and for the XC potential $V_{\mathrm{XC}}^{\mathrm{QNA}} = \delta E_{\mathrm{XC}}^{\mathrm{QNA}}/\delta n$, which involves higher than first order derivatives, a little higher. In practice, however, these possible discontinuities do not constitute a major problem in typical alloy calculations, because for intermetallic compounds and alloys the Voronoi-boundaries lie in the interstitial region where the density gradient is small and all subsystem functionals reduce to LDA, which makes the superposition effectively continuous.

Figure 1 shows the calculated EMTO-CPA equilibrium volumes of disordered Fe-V and V-W binary alloys. QNA produces improved volumes on the whole concentration range by improving the description of the pure elements at the end points. It can be seen that in the case of V-W this means that also the experimental slope of the volume vs. V concentration curve is recovered. It should be noted that while PBE and PBEsol [49] GGA functionals produce different volumes for the V-W alloy, the volume vs. V concentration slope is incorrect and practically identical between the two functionals. The slope having the same incorrect value for both PBE and PBEsol reflects the difficulty of being able to describe V and W with equal accuracy on the GGA level and is connected to the phenomenon of poor GGA-level formation energies of metallic compounds and alloys.

3.2 PBE0 and HSE hybrid functionals

Hybrid functionals, such as HSE and PBE0, typically mix some fraction of Hartree-Fock type exact exchange with existing DFT XC approximations. Such a procedure has been shown to lead to significantly better accuracy than GGAs [50]. Although hybrid functionals are not as popular in solid state physics as they are in chemistry, recently it was shown that intermetallic compounds also benefit from the inclusion of exact exchange [6]. The PBE0 hybrid is a simple modification of the PBE functional in which a quarter of the PBE exchange is replaced with exact exchange. The total PBE0 XC energy is therefore written as

$$E_{\mathrm{XC}}^{\mathrm{PBE0}} = \frac{1}{4}E_{\mathrm{x}}^{\mathrm{HF}} + \frac{3}{4}E_{\mathrm{x}}^{\mathrm{PBE}} + E_{\mathrm{c}}^{\mathrm{PBE}}. \qquad (2)$$

The choice of one quarter is not arbitrary, but yields accurate atomization energies of molecules based on Görling-Levy perturbation theory [19].

The HSE is similar to PBE0, but exchange is split into short- and long-range components as

$$\begin{aligned} E_{\mathrm{XC}}^{\mathrm{HSE}} =& a E_{\mathrm{x}}^{\mathrm{HF,SR}}(\omega) + (1-a) E_{\mathrm{x}}^{\mathrm{PBE,SR}}(\omega) \\ &+ E_{\mathrm{x}}^{\mathrm{PBE,LR}}(\omega) + E_{\mathrm{c}}^{\mathrm{PBE}}, \end{aligned} \qquad (3)$$

where ω is a range parameter and a gives the fraction of exact exchange that should be mixed with the PBE exchange. In this paper by HSE we mean the HSE06 variant for which $\omega = 0.2$ and $a = 1/4$. With parameters $\omega = 0$ and $a = 1/4$ HSE reduces to PBE0. The benefit of the HSE functional is that for large systems it is computationally significantly less demanding than PBE0.

4 The Cu-Au intermetallic compound

4.1 Formation energies

Figure 3 shows the formation energies of the Cu_3Au-$L1_2$, CuAu-$L1_0$, $CuAu_2$-β_2, and $CuAu_3$-$L1_2$ phases. The present calculations, except VASP PBE, were performed non-self-consistently by either running one iteration starting from self-consistently relaxed VASP PBE structures

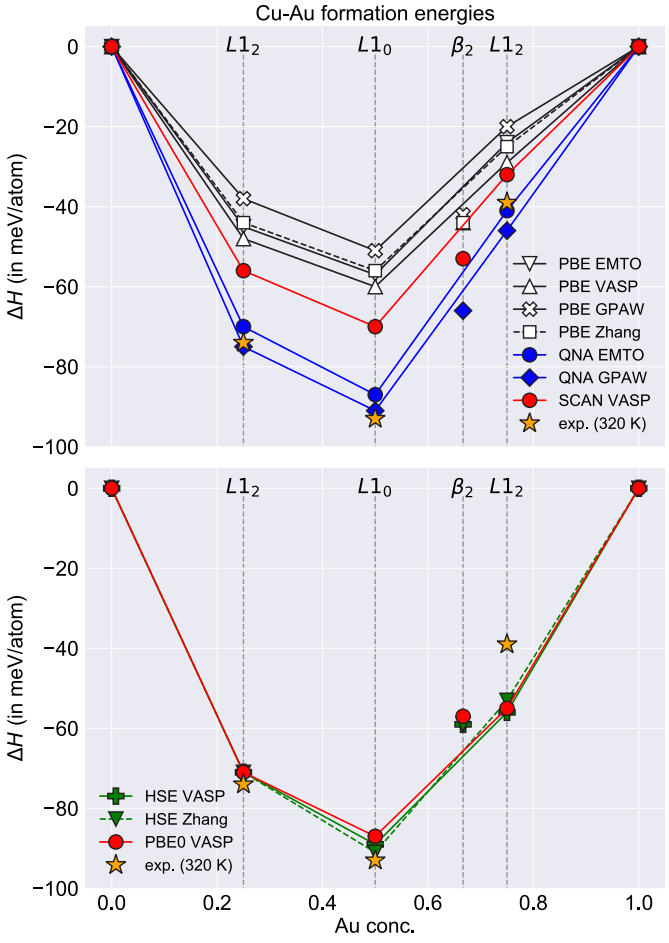

Fig. 3. Non-self-consistent Cu-Au formation energies for PBE, QNA, and SCAN (upper panel) and PBE0, and HSE (lower panel) using self-consistently relaxed PBE geometries. Self-consistent VASP PBE Zhang and HSE Zhang and experimental values are taken from reference [6]. Non-self-consistent PBE and QNA EMTO data are taken from reference [8].

and wavefunctions (VASP HSE and PBE0) or evaluating the total energy using self-consistently calculated PBE density using VASP PBE structures (GPAW QNA), but in both cases calculations were performed for static VASP PBE geometries without optimizing the geometry for each functional. The figure also shows EMTO PBE and QNA calculations from reference [8], which are also non-self-consistent, but those calculations evaluate the total energy using self-consistent LDA densities and for them also the total energy was minimized by equation of state fitting. Fully self-consistent VASP PBE and HSE data, which are also shown, are taken from reference [6].

As has been established, PBE formation energies are far from the experimental values, and the $CuAu_2$-β_2 is predicted to be stable and $CuAu_3$-$L1_2$ unstable. As a quantity the formation energy here seems not to be very sensitive to the details of the calculations. This is evidenced by the fact that the different PBE datasets in Figure 3 agree very well despite them being based on different combinations of DFT codes and non-self-consistent treatments. We have also tried the SCAN meta-GGA [51] in a one-iteration manner similar to the HSE and PBE0 calculations. We see that SCAN is able to improve the formation energies to some extent, but the stable $CuAu_2$-β_2 phase remains. Even better accuracy is achieved with QNA, which for Cu_3Au-$L1_2$ and CuAu-$L1_0$ produces formation energies that agree almost perfectly with those of the hybrids and experiments. Despite the excellent performance for the Cu-rich side, the Au-rich side is more questionable because the $CuAu_2$-β_2 phase is still predicted to be stable, although the margin by which the β_2 phase is stable is narrower for QNA than it is for PBE or SCAN.

The lower panel of Figure 3 shows the formation energies of the HSE and PBE0 hybrid functionals. We confirm the excellent performance of these hybrids, which was first reported by Zhang et al. [6] who used the HSE functional. It can be seen that the lack of self-consistency changes the HSE formation energies very little compared to the fully self-consistent HSE formation energies from reference [6]. Furthermore, the non-self-consistent one-iteration treatment is enough to keep the qualitatively correct phase stability intact. We also notice that HSE and PBE0 predict almost identical formation energies, which could indicate that Cu-Au is not very sensitive to the screening length details of the HSE functional. For example, Co-Pt has been reported to be a problematic system for HSE due to the unsuitability of the standard HSE screening length for Co [7]. The above findings suggest that one-iteration hybrids can be a viable alternative to the much slower fully self-consistent hybrid calculations, at least for the properties and the type of systems considered here.

4.2 Electronic densities of states

An interesting observation is that QNA and HSE/PBE0 agree almost perfectly on the Cu-rich side, but the Au-rich side shows the qualitative disagreement in the phase stability. This suggests that the correct phase stability on the Au-rich side depends on nonlocal exchange effects, which are not described by GGA or meta-GGA level approximations. In order to confirm this, we plot the electronic densities of states (DOS) in Figure 4. The left panels of Figure 4 show the total DOS of PBE, QNA, and PBE0 functionals. The DOS calculations used the same self-consistently relaxed VASP PBE geometries as the formation energy calculations of Figure 3. The PBE and PBE0 DOS are calculated with VASP and the QNA DOS with GPAW.

The PBE and PBE0 DOS are in good agreement with those of reference [6]. It can be seen that the DOS changes very little between PBE and QNA functionals when they are calculated using same input geometries. The same is true between PBE0 and HSE (not shown) DOS curves. When comparing PBE0 and GGA-level DOS curves, however, PBE0 DOS shows a shift toward lower energies, which is a consequence of the (partial) removal of the self-interaction error [4] in the PBE0 functional. This shift alone might not be enough to explain the superior hybrid-level formation energies, because QNA formation energies on the Cu-rich side are comparable to those of hybrids, but the QNA DOS is almost identical to that of PBE.

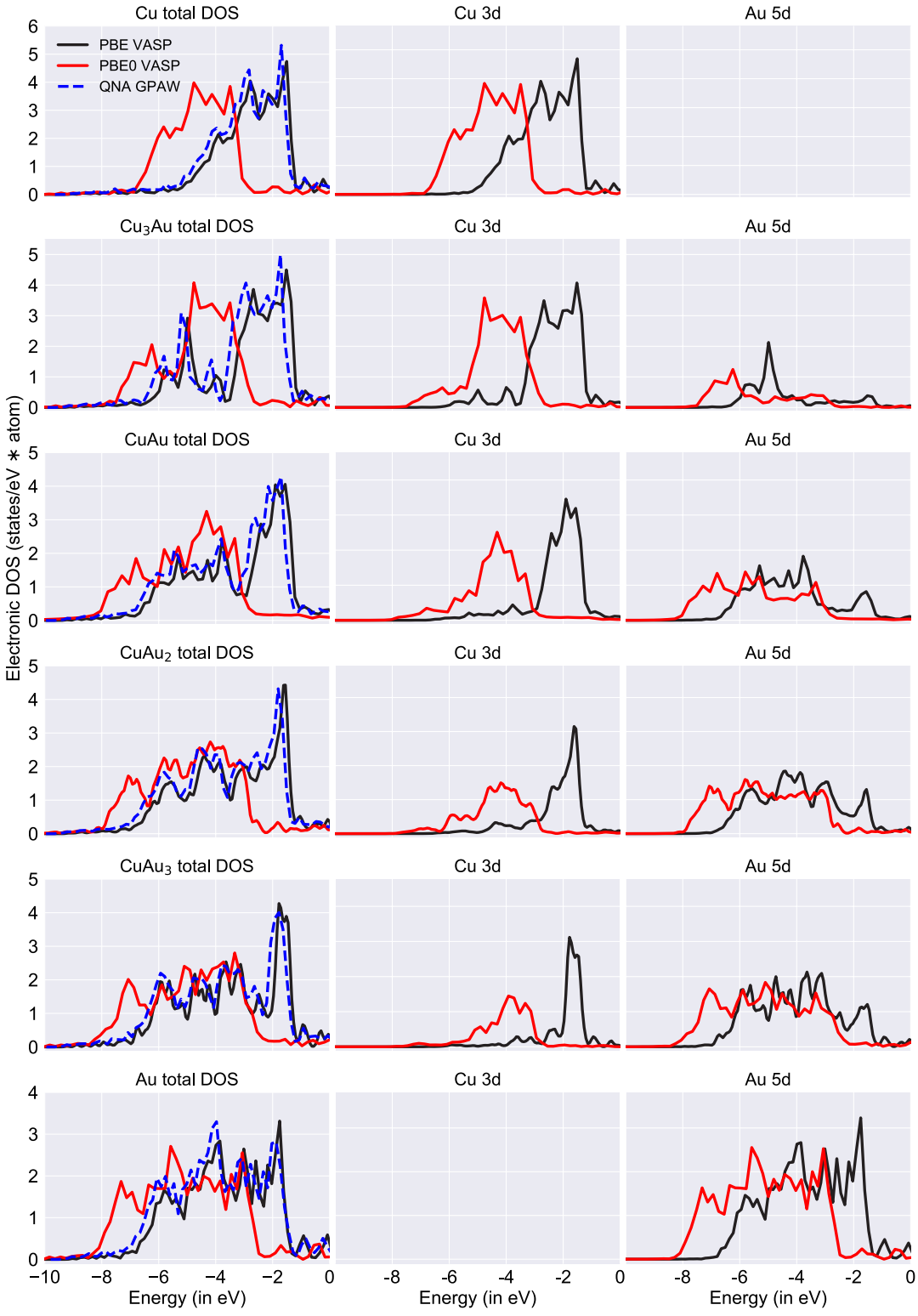

Fig. 4. Electronic densities of states (DOS) of the Cu-Au system using PBE, QNA, and PBE0 functionals. Left panels show the total DOS, middle panels the Cu DOS of the 3*d* electrons, and right panels the Au DOS of the 5*d* electrons. For each functional the DOS was calculated using self-consistently relaxed PBE geometries. In each panel the Fermi level of each DOS curve has been aligned at zero eV.

If we focus instead on the shapes of the DOS curves we can identify some key differences. For Cu, Au, Cu_3Au, and CuAu the GGA and hybrid DOS curves have fairly similar shapes, but $CuAu_2$ and $CuAu_3$ show important changes. We notice that for $CuAu_2$ and $CuAu_3$ the peak in Cu 3*d* DOS vanishes in the PBE0 DOS, which is due to *d*-*d* hybridization between Cu 3*d* and Au 5*d* orbitals. We can also see that the hybridization mainly influences Cu 3*d* DOS, and the Au 5*d* DOS, apart from the shift, remains very similar between PBE0 and PBE/QNA. The hybridization effect is also weakly present in CuAu, but so weakly that it does not seem to affect the formation energy noticeably. Based on the above findings we claim that in order to reproduce the experimentally observed phase stability trends in the Cu-Au system the inclusion of *d*-orbital hybridization is essential.

5 Conclusions

We have calculated the formation energies and electronic densities of states using GGA-, meta-GGA- and hybrid-level XC approximations. GGA and meta-GGA levels are plagued by the presence of a stable $CuAu_2$-β_2 phase, which has never been witnessed experimentally. Hybrid functionals are needed to destabilize the β_2 phase, because the stability of the β_2 phase on GGA and meta-GGA levels is caused by the missing *d*-orbital hybridization.

QNA scheme is shown to be able to produce the most accurate GGA-level formation energies. On the Cu-rich side the QNA results are competitive with hybrid PBE0 and HSE results, but on the Au-rich side QNA and the hybrids have the β_2 phase stability disagreement. Both approaches have their own upsides and downsides. QNA formation energies are excellent for GGA-level, but the stable $CuAu_2$-β_2 remains. Hybrid functionals are able to correct the phase stability by making $CuAu_2$-β_2 unstable, but the use of hybrids comes with a considerable increase in computational cost. Some of this high computational cost can, however, be eliminated by performing only one iteration in the hybrid calculations, which we have seen to be enough to reproduce self-consistent hybrid results.

We acknowledge the Swedish Research Council (VR), the Swedish Foundation for Strategic Research (SSF), the Swedish Foundation for International Cooperation in Research and Higher Education (STINT), the Carl Tryggers Foundations, the Swedish Governmental Agency for Innovation Systems (VINNOVA), the Swedish Energy Agency (Energimyndigheten) and the Hungarian Scientific Research Fund (research project OTKA 109570) for financial support. The computer resources of the Finnish IT Center for Science (CSC) and the FGCI project (Finland) are acknowledged.

Author contribution statement

All the authors were involved in the preparation of the manuscript. All the authors have read and approved the final manuscript.

References

1. P. Hohenberg, W. Kohn, Phys. Rev. **136**, B864 (1964)
2. W. Kohn, L.J. Sham, Phys. Rev. **140**, A1133 (1965)
3. R.M. Dreizler, E.K.U. Gross, *Density functional theory* (Springer-Verlag, Berlin, Heidelberg, 1990)
4. A.J. Cohen, P. Mori-Sánchez, W. Yang, Chem. Rev. **112**, 289 (2012)
5. V. Ozoliņš, C. Wolverton, A. Zunger, Phys. Rev. B **57**, 6427 (1998)
6. Y. Zhang, G. Kresse, C. Wolverton, Phys. Rev. Lett. **112**, 075502 (2014)
7. E. Decolvenaere, M.J. Gordon, A. Van der Ven, Phys. Rev. B **92**, 085119 (2015)
8. L.Y. Tian, H. Levämäki, M. Ropo, K. Kokko, Á. Nagy, L. Vitos, Phys. Rev. Lett. **117**, 066401 (2016)
9. S.H. Vosko, L. Wilk, M. Nusair, Can. J. Phys. **58**, 1200 (1980)
10. J.P. Perdew, Y. Wang, Phys. Rev. B **45**, 13244 (1992)
11. J.P. Perdew, K. Burke, M. Ernzerhof, Phys. Rev. Lett. **77**, 3865 (1996)
12. D.C. Langreth, M.J. Mehl, Phys. Rev. B **28**, 1809 (1983)
13. A.D. Becke, Phys. Rev. A **38**, 3098 (1988)
14. J.P. Perdew, J.A. Chevary, S.H. Vosko, K.A. Jackson, M.R. Pederson, D.J. Singh, C. Fiolhais, Phys. Rev. B **46**, 6671 (1992)
15. J. Heyd, G.E. Scuseria, M. Ernzerhof, J. Chem. Phys. **118**, 8207 (2003)
16. J. Heyd, G.E. Scuseria, M. Ernzerhof, J. Chem. Phys. **124**, 219906 (2006)
17. H. Levämäki, M.P.J. Punkkinen, K. Kokko, L. Vitos, Phys. Rev. B **86**, 201104 (2012)
18. H. Levämäki, M.P.J. Punkkinen, K. Kokko, L. Vitos, Phys. Rev. B **89**, 115107 (2014)
19. J.P. Perdew, M. Ernzerhof, K. Burke, J. Chem. Phys. **105**, 9982 (1996)
20. M. Ernzerhof, G.E. Scuseria, J. Chem. Phys. **110**, 5029 (1999)
21. G. Kresse, J. Hafner, Phys. Rev. B **47**, 558 (1993)
22. G. Kresse, J. Furthmüller, Comput. Mater. Sci. **6**, 15 (1996)
23. G. Kresse, J. Furthmüller, Phys. Rev. B **54**, 11169 (1996)
24. J.J. Mortensen, L.B. Hansen, K.W. Jacobsen, Phys. Rev. B **71**, 35109 (2005)
25. J. Enkovaara et al., J. Phys. Condens. Matter **22**, 253202 (2010)
26. P.E. Blöchl, Phys. Rev. B **50**, 17953 (1994)
27. G. Kresse, D. Joubert, Phys. Rev. B **59**, 1758 (1999)
28. H.J. Monkhorst, J.D. Pack, Phys. Rev. B **13**, 5188 (1976)
29. O.K. Andersen, O. Jepsen, G. Krier, Exact muffin-tin orbital theory, in *Lectures on methods of electronic structure calculations*, edited by V. Kumar, O.K. Andersen, A. Mookerjee (World Scientific, Singapore, 1995), January 1994, pp. 63–124
30. L. Vitos, I.A. Abrikosov, B. Johansson, Phys. Rev. Lett. **87**, 156401 (2001)

31. L. Vitos, Phys. Rev. B **64**, 014107 (2001)
32. L. Vitos, *Computational quantum mechanics for materials engineers*, Engineering materials and processes (Springer London, London, 2007)
33. R.M. Martin, *Electronic structure: basic theory and practical methods* (Cambridge University Press, Cambridge, 2005)
34. P. Soven, Phys. Rev. **156**, 809 (1967)
35. B.L. Györffy, Phys. Rev. B **5**, 2382 (1972)
36. L. Vitos, J. Kollár, H.L. Skriver, Phys. Rev. B **55**, 13521 (1997)
37. J. Kollár, L. Vitos, H. Skriver, in *Electronic structure and physical properies of solids* (Springer Berlin Heidelberg, Berlin, Heidelberg, 1999), pp. 85–114
38. A. Östlin, L. Vitos, L. Chioncel, Phys. Rev. B **96**, 125156 (2017)
39. H. Levämäki, Developing exchange-correlation and kinetic energy functional approximations for density functional theory, University of Turku, 2018
40. P. Haas, F. Tran, P. Blaha, K. Schwarz, R. Laskowski, Phys. Rev. B **80**, 195109 (2009)
41. G.I. Csonka, J.P. Perdew, A. Ruzsinszky, P.H.T. Philipsen, S. Lebègue, J. Paier, O.A. Vydrov, J.G. Ángyán, Phys. Rev. B **79**, 155107 (2009)
42. M. Fuchs, M. Bockstedte, E. Pehlke, M. Scheffler, Phys. Rev. B **57**, 2134 (1998)
43. A. Zupan, P. Blaha, K. Schwarz, J. Perdew, Phys. Rev. B **58**, 11266 (1998)
44. A.V. Ruban, I.A. Abrikosov, Rep. Prog. Phys. **71**, 046501 (2008)
45. W. Kohn, A.E. Mattsson, Phys. Rev. Lett. **81**, 3487 (1998)
46. R. Armiento, A. Mattsson, Phys. Rev. B **66**, 1 (2002)
47. A.E. Mattsson, R. Armiento, Int. J. Quantum Chem. **110**, 2274 (2010)
48. F. Hao, R. Armiento, A.E. Mattsson, Phys. Rev. B **82**, 115103 (2010)
49. J.P. Perdew, A. Ruzsinszky, G.I. Csonka, O.A. Vydrov, G.E. Scuseria, L.A. Constantin, X. Zhou, K. Burke, Phys. Rev. Lett. **100**, 136406 (2008)
50. A.D. Becke, J. Chem. Phys. **140**, 18A301 (2014)
51. J. Sun, A. Ruzsinszky, J.P. Perdew, Phys. Rev. Lett. **115**, 036402 (2015)